7

Triangular Mesh Modelling for Archaeological Applications

H.Suzuki, T.Kanai, Y.Kandori, K.Toki, M.Terasawa[†] *and F.Kimura*
Department of Precision Machinery Engineering
The University of Tokyo
Hongo 7-3-1, Bunkyo, Tokyo 113, Japan
E-mail: suzuki@cim.pe.u-tokyo.ac.jp
[†]*Nihon University, Tokyo, Japan*

Abstract
This paper describes methods for generating triangular mesh models from unorganized measured data points, and also for simplifying the mesh models. These methods are used in the course of a joint research project conducted for "Revival of Neanderthal" at The University of Tokyo for creating three dimensional data base of bones of a Neanderthal man. Using this data base, we also tried many applications for archaeological analyses; assembly of mesh models into a skeleton, bone restoration, gait simulation, growth simulation, and creation of bone replicas with a rapid prototyping technology.

Keywords
Surface Reconstruction, Triangular Mesh Modelling, Mesh Simplification.

1 INTRODUCTION

The Japan-Syria joint investigating team excavated bones of a Neanderthal infant in Dederiyeh cave, Syria in 1993 (Akazawa et al. 1995a,b). The condition of its preservation was extremely good and about two hundred bones remain as shown in Figure 1.

A joint research project was conducted for "Revival of Neanderthal" to give a breath to the Neanderthal man with extensive use of computer graphics technologies. It is an interesting trial to apply computer graphics technologies to morphological analyses in archaeology.

As a key part of this project, our major mission is to build a three dimensional (3D) data base of the bones. In this data base, shapes of bones are represented as triangular mesh models. The major issues are:

- creation of 3D mesh models for bones, and
- simplification of the mesh models.

Using this data base, we tried many applications for archaeological analyses, which include:

M. J. Pratt et al. (eds.), *Product Modeling for Computer Integrated Design and Manufacture*

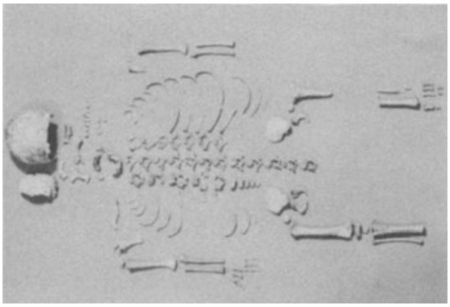

Figure 1 Bones of Dederiyeh Neanderthal Man (Courtesy of Prof. Akazawa, The Univ. of Tokyo, Japan)

- constructing a skeleton from bone mesh models,
- bone restoration,
- gait simulation,
- growth simulation, and
- creation of bone replicas with a rapid prototyping technology.

2 MESH MODEL CREATION

2.1 Measuring Method

The first step for making 3D data base is to measure shapes of bones using a measuring machine. Figure 2 shows a schematic view of the machine, which employs a non-contact, laser scanning method. An object to be measured is clamped to the spindle located on the platform which has two degrees of freedom of motion along X, Y axes. The platform steps forward in the X direction by a specified pitch. At each step laser beam (sheet) spreads onto the object in the Y direction to form a reflected curve on its top surface. The image of the curve is taken by the two CCD cameras and is used to compute Y and Z coordinates of points on the object's surface. The resolution is about 70 μm. The pitch in the X direction is variable, and the minimum of 0.2mm. We call this scanning process "X-scan" for the whole X range of the object.

After finishing one X-scan, the platform returns back to the initial X position and the spindle rotates by 60 degrees around X axis, then another X-scan is made. This process is repeated six times so that the points on the girth of the object can be scanned. In case Y range of the object is beyond the laser scanning scope, the platform takes necessary movement also in the Y direction.

This measurement process is automatically done by the measuring machine. One difficulty is to choose a right clamping position of the object. It is obvious that data is not obtained for such unseen portions that the laser beam cannot reach or the cameras cannot

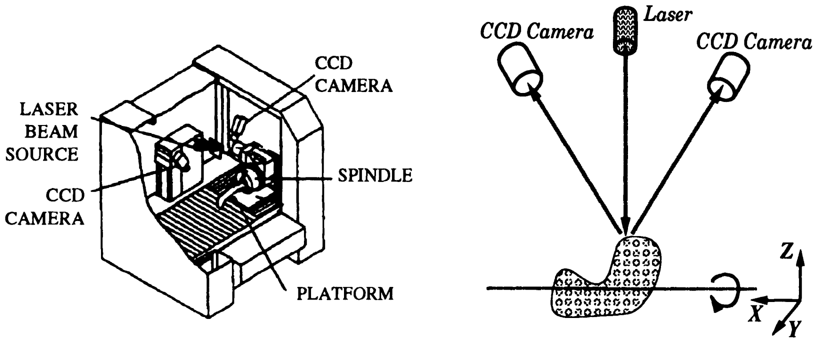

Figure 2 Measurement with 3D Laser Scanning Measuring Machine

observe. Since shapes of bones are not so smooth, we have to be very careful to choose the clamping position.

It is also difficult to properly clamp a bone. It is inevitable that we can not measure portions that are covered by the clamping tool, so it is desirable to minimize such portions. Another constraint for clamping is that any tiny damage to the bones is not allowed, because they are extremely precious. Our practical solution is to glue a thin handle to a bone and clamp this handle. By using this method, the unmeasurable area is relatively small compared to other clamping methods.

2.2 Mesh Creation

From a cloud of points obtained by the measurement, a triangular mesh model is created. Various kinds of methods have been proposed for creating a mesh from a set of unorganized points. Our method is categorized to be an implicit function reconstruction method and based on method proposed by Hoppe (1992). It consists of three procedures:

1. generate a potential field around data points,
2. create a mesh as an isosurface of the potential field using Marching Cube Algorithm (Lorensen, 1987), and
3. refine the mesh to be closer to the data points.

We assume voxels arranged in a 3D lattice ($N_x \times N_y \times N_z$) that covers all the data points. The objective is to define such a potential value at each of the voxels that is positive if the voxel is inside the object and negative if it is outside the object. Then the mesh can be defined as the zero isosurface of this potential field.

Here we briefly introduce Hoppe's method. In order to generate a potential field, some number of near-by points are grouped to form a neighborhood, then its center point and normal vector are defined. After a set of the neighborhoods covering all the data points are defined, the center points of close neighborhoods are connected to form a graph. Using this graph, the directions of the normal vectors of the neighborhoods are adjusted to be consistent to each other. Based on those neighborhoods, a potential field is defined to be the signed distance from a point to its nearest neighborhood.

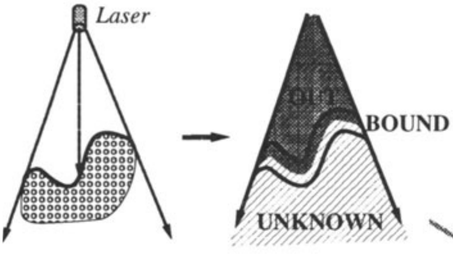

Figure 3 Classification of Lattice Points

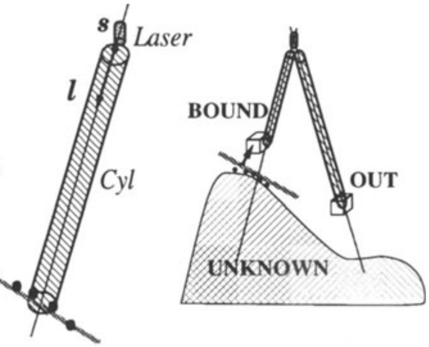

Figure 4 Potential Field Computation

From our experience, this method is robust and works well in many cases particularly for smooth surfaces. However, for such an object as our bones of irregular shapes, the neighborhoods cannot be always defined in a good condition. Specifically, when a bone has a sharp thin edge, it seems difficult to define proper neighborhoods for the points around the tip of the edge. The neighborhoods in such a region are sensitive to the choice of data points for defining the neighborhoods. Thus the method tends to generate a potential field of an unexpected shape.

Our approach is influenced by the idea of the hole filling algorithm by Curless (1996), in which the optical configuration of the measuring machine is taken into account for generating a potential field. Hereafter let's consider the data points obtained by one X-scan. As shown in Figure 3, it is apparent that the space between the laser source and a data point is empty. This means that the voxels between the laser source and the data point are outside the object and those including the data points are on the boundary of the object. These outside voxels are labeled "OUT" and those on the boundary are labeled "BOUND." And the voxels behind the data points can be inside or outside the object, so they are labeled "UNKNOWN." In Figure 4, in order to determine the potential values of these voxels, we extend a cylinder l from the laser source s toward the voxels until it hits some data points or reaches out of the lattice. In the latter case a large negative potential value is assigned to the voxels on this cylinder. In the former case a neighborhood similar to Hoppe's is defined, and the signed distance from each of the voxels on this cylinder to the neighborhood is computed as its potential value. Thus the potential field for the data points from a single X-scan is obtained.

As mentioned above, the scanning process consists of six X-scans from six different directions. We generate six potential fields for these X scans. These potential fields are averaged to form the total potential field as shown in Figure 5. The labels of voxels are also used for averaging. Then the Marching Cube Algorithm is used to generate a mesh.

An example is shown in Figure 6, 7 and 8. The range of data points in X direction is about 150mm and the scanning pitch is 0.5mm. The lattice is 56×67×64 and its gap is 2.5mm. Figure 6 shows a set of data points obtained by measuring the skull from its front side. The number of the data points is 10,463. The picture on right hand side shows voxels with positive potential values.

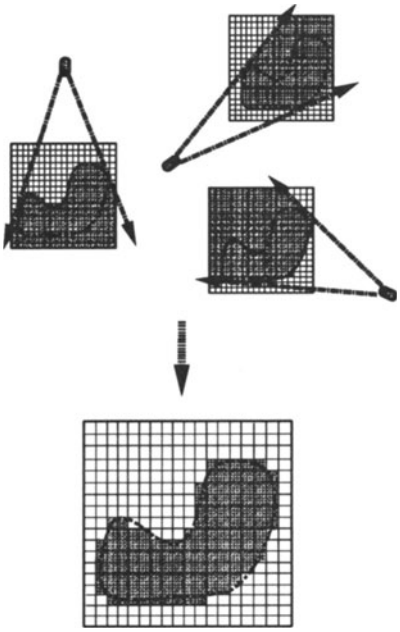

Figure 5 Merging Potential Fields of Multiple X-Scans

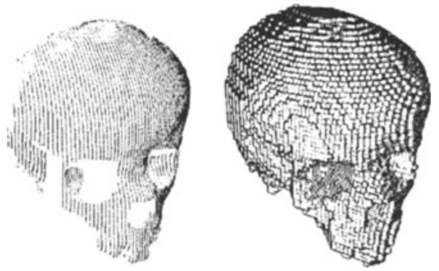

Figure 6 Left: Data Points for a Single Scan (10,463 points) and Right: Voxels with Positive Potential Value

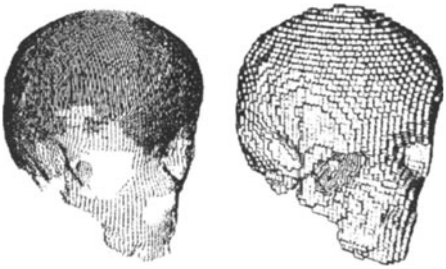

Figure 7 Left: The Whole Data Points (36,722 points) and Right: Voxels with Positive Potential Value

Figure 7 shows the whole data points whose number is 36,722 and the positive voxels in the merged potential field. These data points are the sum of those obtained by six X-scans with approximately duplicated points being merged. The mesh generated using the Marching Cube Algorithm is shown in Figure 8. It includes 45,348 faces.

Comparing Figure 8 and the data points shown in Figure 7, the generated mesh is apparently not smooth and exhibits aliasing artifacts. The mesh can be improved by using a finer lattice with smaller gaps, but it is computationally expensive. In our approach a mesh fairing procedure is carried out. More specifically, positions of the vertices of the mesh are adjusted to minimize the distance from the data points. Figure 9 shows the mesh obtained by fairing the mesh in Figure 8.

The total computation time for this example is about 2 minutes on Sun SparcStation 20, most of which is spent on generating the potential field.

2.3 Mesh Simplification

Usually a mesh generated for a bone contains about 10^4 to 10^5 faces. In some applications discussed later in this paper, we need the whole skeleton of about 80 pieces of bones. So

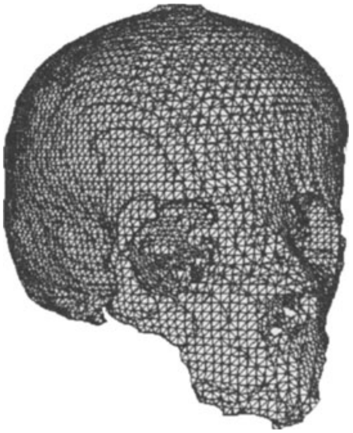

Figure 8 Triangular Mesh Generated with Marching Cube Algorithm (45,384 faces)

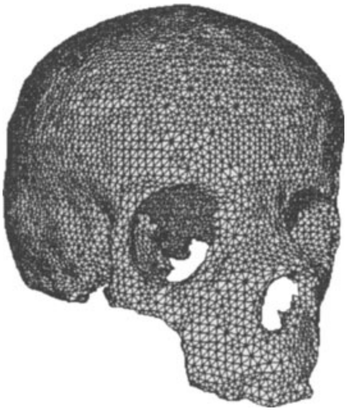

Figure 9 Refined Mesh Model

the number of the triangular faces in the skeleton adds up to the order of 10^6 which is too large to be processed on a desk top workstation. And it is also true that for some applications, we do not need such a fine mesh.

The mesh simplification is a process to reduce the number of faces while keeping the topological, geometrical characteristics of the original mesh. We use an excellent method proposed by Hoppe (1993). In his method, an energy function E is defined for a mesh:

$$E = E_{dist} + E_{spring} + E_{rep}$$

where E_{dist} represents the total of the distances between the mesh and data points, and E_{spring} is the total of elastic energy of springs virtually connecting vertices of the mesh. E_{rep} is proportional to the number of the vertices, that is,

$$E_{rep} = C_{rep}m \tag{1}$$

where C_{rep} is a constant and m is the number of the vertices.

The simplification is made by minimizing E by changing the positions of the vertices of the mesh, and also by applying local edge operations shown in Figure 10 for deleting vertices or changing the graph structure of the mesh. A "generation and test" type algorithm is proposed for finding an optimal solution. This algorithm is excellent, although it takes large computation time.

We implemented and applied this algorithm for simplifying meshes, which are then used by applications described in the succeeding section. One requirement for the simplification arises from the application of the skeleton assembly explained in Section 3.1. In order to assemble pieces of bones, anatomists have to refer to key shape features of the bones. In

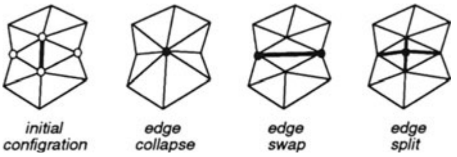

Figure 10 Local Edge Operations (Hoppe, 1993)

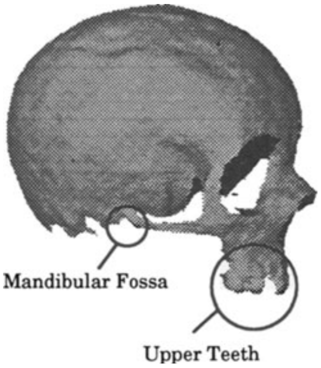

Figure 11 Key Features for Assembling Skull and Jaw

Figure 11, two key features are shown, which are used for assembling the skull and the jaw.

Portions of the mesh representing such key features must not be simplified. We introduce weight w_i to the ith vertex and rewrite E_{rep} in (1) to

$$E_{rep} = C_{rep} \sum_i w_i,$$

where w_i ranges from 0 to 1. In case all w_is are 1, E_{rep} is identical to (1). Vertices with smaller w_i will more possibly remain without getting eliminated.

Figure 12 shows the result of Hoppe's simplification of the mesh in Figure 9. The number of the faces is reduced to 874, which is about 2% of the original mesh. Figure 13 shows the result of weighted simplification, where the weights of the vertices in the circles shown in Figure 11 are set to be zero. It can be seen that the triangles in these circles are preserved compared to Figure 12. The number of faces is 1397. The computation time is about 8 hours on Sun SparcStation 20.

3 ARCHAEOLOGICAL APPLICATIONS

Once building up 3D data base of bones, we can apply computer graphics technologies to making various analyses which have been impossible for conventional archaeological methodologies. We tried and developed many applications introduced in this section.

3.1 Skeleton Assembly

Simplified mesh models for bones are assembled into a skeleton. An anatomist used a data visualization tool, SGI Inventor, to manually assemble the bone mesh models into a

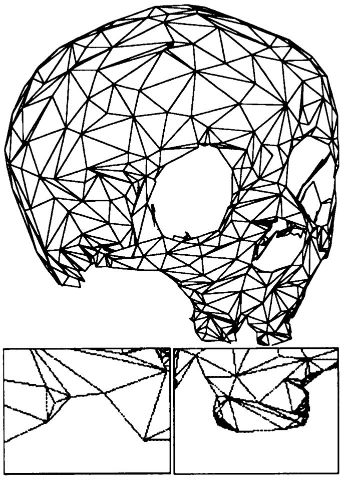

Figure 12 Mesh Simplification with Equal Weights (874 faces). Bottom: Magnified View of the Triangles in the Circles of Figure 11.

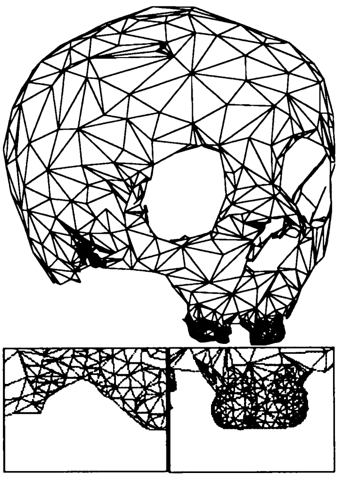

Figure 13 Local Control of Mesh Simplification (1,397 faces). Bottom: Magnified View of the Triangles in the Circles of Figure 11.

skeleton. The assembly task requires such expertise that it seems very difficult to realize an automatic assembly.

Because of the mesh simplification, response of the workstation is fast enough for the anatomist to interactively adjust the positions of the bones. Figure 14 shows the complete skeleton. The skeleton includes the total of 140,512 faces in 78 bone mesh models.

3.2 Mesh Restoration

It must be noted that the excavated skeleton had lost many bones and many of them had been broken, although it is much more complete than is often the case. Some missing portions are physically recovered by an anatomist, for instance, by adding wax to the broken portions.

In 3D data base, we restore mesh models by mirror imaging. Since bones on the right hand side of the body and those on the left hand side have symmetrical shapes, missing portions can be compensated using their counterparts. Figure 15 shows an example of such compensation. This is a jaw bone whose right half is not complete. The mirror image of the left half replaces with this right half.

3.3 Gait Simulation

A gait simulation enables us to visualize the difference in gait of modern men and of Neanderthal men. The motion is computed by one of our project partners from Keio

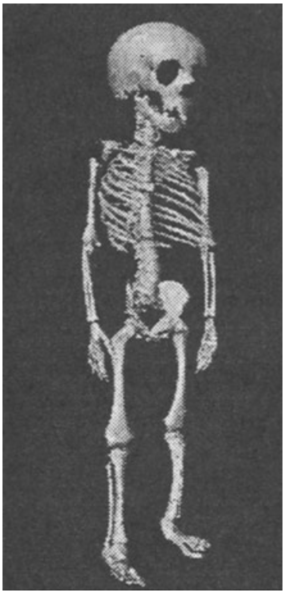

Figure 14 Complete Skeleton (78 bone mesh models of 140,512 faces)

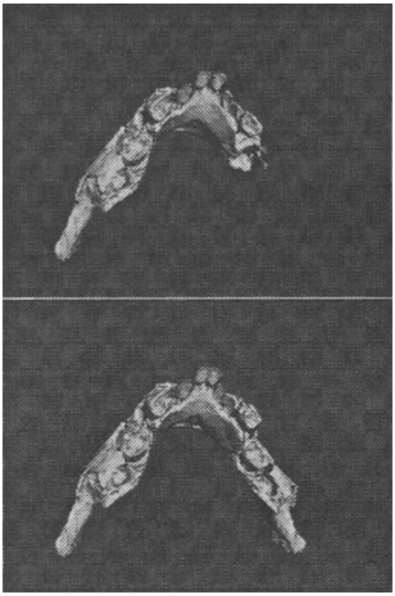

Figure 15 Restoration of Lower Jaw Bone. Upper: Broken Bone and Lower: Restoration by Mirroring

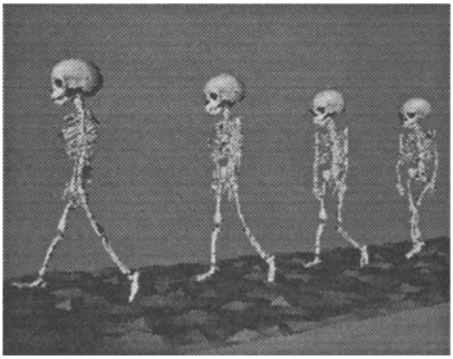

Figure 16 Gait Simulation

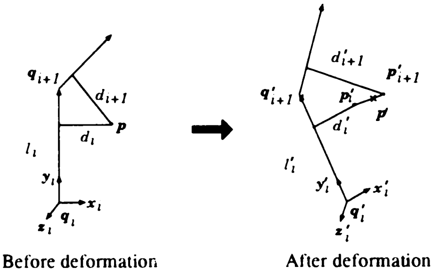

Figure 17 Control Lines for 3D Morphing

University using a simplified structural model for dynamic behavior of gait. The computed motion data was applied to our skeleton model as shown in Figure 16.

3.4 Growth Simulation

Another application is a growth simulation. The Dederiyeh Neanderthal is estimated to be 1.7 years old. We make him/her grow up to be an adult (20 years old) by taking into account different growth rates of different portions of the bone. We simulate only the growth of the skull.

In order to modify the shape of the mesh model for the skull, we extend the two dimensional morphing technique proposed by Beier (1992) to the 3D space. Positions of the vertices of the mesh model are modified according to the control lines as shown in Figure 17. First, for each control line l_i, we define a local coordinate system of which origin is $\boldsymbol{q}_i$ and of which axis vectors are $\boldsymbol{x}_i, \boldsymbol{y}_i, \boldsymbol{z}_i$. The control lines are connected to be a polyline in order to define the positions of the axes. The local coordinates $\boldsymbol{u}_i$ of $\boldsymbol{p}$ is:

$$\boldsymbol{u}_i = \frac{1}{|l_i|}(\boldsymbol{p} - \boldsymbol{q}_i)^T \begin{pmatrix} \boldsymbol{x}_i \\ \boldsymbol{y}_i \\ \boldsymbol{z}_i \end{pmatrix}$$

where $|l_i|$ is the length of l_i. By transforming $\boldsymbol{p}$ from l_i to l'_i, $\boldsymbol{p}'_i$, the new position of $\boldsymbol{p}$ in terms of l_i, is defined with $\boldsymbol{u}_i$ as follows:

$$\boldsymbol{p}'_i = |l'_i|\ \boldsymbol{u}_i{}^T \begin{pmatrix} \boldsymbol{x}'_i \\ \boldsymbol{y}'_i \\ \boldsymbol{z}'_i \end{pmatrix} + \boldsymbol{q}'_i$$

Finally new position $\boldsymbol{p}'$ is given as the weighted sum of those $\boldsymbol{p}_i$s:

$$\boldsymbol{p}' = \frac{1}{W}\sum_i w_i \boldsymbol{p}'_i \qquad w_i = (1 + \frac{|d_i|}{|l_i|})^{-n_i} \qquad W = \sum_i w_i$$

where $|d_i|$ is the distance between $\boldsymbol{p}$ and l_i and n_i is a constant to specify the range of influence of l_i.

Two sets of control polylines are defined, one for the Dederiyeh Neanderthal man and the other for an adult Neanderthal man named "Amud" as shown in Figure 18. They are defined by an anthropologist. Those control polylines are connecting so called characteristic points as shown in Figure 19. These characteristic points change their positions as the growth. Their intermediate positions between the age of 2 and 19 are estimated with an anthropological technique using the growth data for modern American Caucasians. Thus the sets of control polylines for the intermediate states at each age between 2 and 19 are defined. Linear interpolation between every two successive sets of these control polylines are also made for making growth animation.

Figure 20 shows the result of the simulation. One characteristic of a skull of an adult Neanderthal man is its prominent supraorbital torus, which an infant does not have. The simulation shows how the supraorbital torus come out as the growth proceeds.

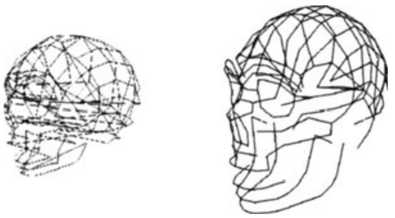

Figure 18 Control Polylines for Dederiyeh Neanderthal (left) man and Amud (right)

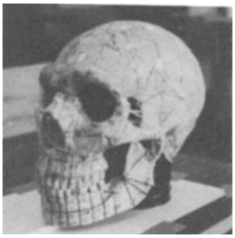

Figure 19 Characteristic Points Specified for Amud (Courtesy of Dr. M. Kouchi, National Institute of Bioscience and Human-Technology, Japan)

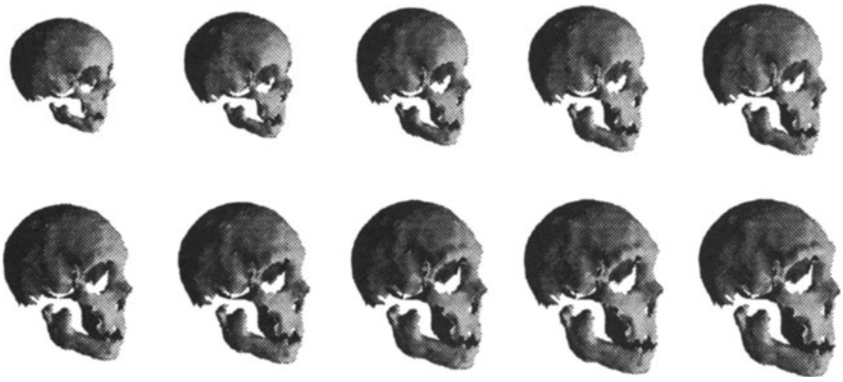

Figure 20 Growth Simulation (from left to right, top to bottom, ages of every 2 years from 2 to 20)

3.5 Rapid Prototyping of Bone Replicas

We use a stereolithography machine to create replicas of bones automatically from mesh models. Figure 21 shows a plastic model of a hand. It gives us a handy, fast and cheaper way to make replicas of fossils than by hand works. These replicas are used for making a plastic skeleton by connecting them. Then the outer skin of Dederiyeh Neanderthal man was also restored by putting clay onto the plastic skeleton.

4 CONCLUSIONS

This paper describes a joint research project conducted for "Revival of Neanderthal." As a part of this project, we built a 3D data base of bones of the Dederiyeh Neanderthal man. In this data base, shapes of the bones are represented as triangular mesh models. We proposed a method to create these mesh models from a set of measured data points, and a method for mesh simplification.

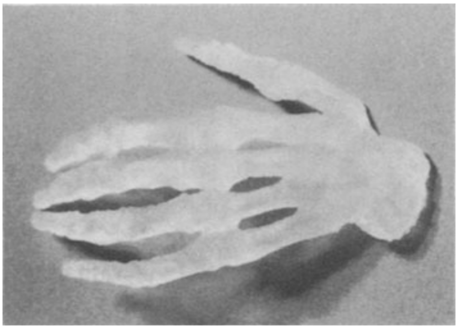

Figure 21 Rapid Prototyping with Stereolithography

Using this data base, we tried many applications for archaeological analyses; assembly of mesh models into a skeleton, gait simulation, growth simulation, and creation of bone replicas with a rapid prototyping technology.

Those applications have attracted the archaeologists very much and indicated the further possibility of computer graphics technologies to archaeological applications.

ACKNOWLEDGMENTS

This research is a part of the joint project conducted by Prof. T. Akazawa at The University of Tokyo. It also involves members from Nihon University, Tohoku University, Keio University, Tokyo University of Art and Music, National Inst. of Bioscience and Human-Tech., CMET Inc., Unisn Inc., Nabla Co., NHK (Nippon Hoso Kyokai) and Toppan Co. The authors wish to thank for their partnership. Special thanks are due to Prof. Akazawa and Dr. Kouchi for their helpful comments.

REFERENCES

Akazawa, T. et al. (1995a) Neanderthal infant burial, *Nature*, Vol. 377, pp. 585-586.

Akazawa, T. et al. (1995b) Neanderthal infant burial from the Dederiyeh cave in Syria, *Paléorient*, Vol. 21/2, pp. 77-86.

Beier, T. and Neely S. (1992) Feature-based Image Metamorphosis, *ACM Computer Graphics*, Vol. 26, No.2, pp.35-42.

Hoppe, H. et al. (1992) Surface Reconstruction from unorganized points, *ACM Computer Graphics,* Vol. 26, No. 2, pp. 71-78.

Hoppe, H. et al (1993) Mesh Optimization, *Proc. of ACM SIGGRAPH '93,* pp.19-26.

Curless, B. and Levoy, M. (1996) A Volumetric Method for Building Complex Meshes from Range Images, *to appear in ACM SIGGRAPH '96.*

Lorensen, W.E. et al. (1987) Marching Cubes: 3D Surface Construction Algorithm, *ACM Computer Graphics,* Vol. 21, No.4, pp.163-169.

More information about the project is available under the homepage:
`http://www.cim.pe.u-tokyo.ac.jp/`